Supporting Information

Self-Healing Redox Chemistry in Cu–TiO_2 Photocatalysts for Enhanced Hydrogen Production

Mariyum Yousaf[1], Hui Hu[1], Faheem Abbas[3], Xuxing Chen[1], Yongge Wei[3], Muhammad Sohail*[2], Yun Gao*[1].

[1]*Ministry of Education Key Laboratory for the Green Preparation and Application of Functional Materials, School of Materials Science & Engineering, Hubei University, Wuhan, Hubei 430062, People's Republic of China*

[2]*Department of Natural Sciences, Faculty of Science and Engineering, Manchester Metropolitan University, Manchester M15 6BX, United Kingdom*

[3]*Department of chemistry, key lab of organic optoelectronics and Molecular Engineering of Ministry of Education, Tsinghua University, Beijing, 100084, PR China*

Corresponding Authors: Email: gaoyun@hubu.edu.cn, muhammad.Sohail@mmu.ac.uk

Table of Contents

S1. Experimental details

Materials

Titanium butoxide ($C_{16}H_{36}O_4Ti$) and Hydrofluoric acid (HF AR,>40%) were bought from Shanghai Aladdin biochemical technology co., Ltd. (China). Absolute ethanol (C_2H_6O) Methanol (CH_4O), and Sodium hydroxide (NaOH) were purchase from the Sinopharm chemical reagent co., Ltd. (China. Precursor Copper (II) nitrate tri-hydrate, $Cu(NO_3)_2.3H_2O$, 99%) bought from Innochem co., Ltd. (China). All the chemicals used directly without further purification. Ultra-pure and DI water used throughout this experiment.

Synthesis of Catalyst

Template-free Cu–doped TiO_2 (Cu–TiO_2) photocatalysts were synthesized using a one–step hydrothermal method. First, 20 mL of Titanium Butoxide [$Ti(OBu)_4$] was placed in a 100 mL beaker, followed by the dropwise addition of 2 mL Hydrofluoric acid (HF) under continuous stirring for 30 minutes. Separately, $Cu(NO_3)_2 \cdot 3H_2O$ (ranging from 0.5 to 14 wt%) was dissolved in 50 mL of deionized (DI) water and ultra-sonicated for 10 minutes until a clear solution was obtained. The two solutions were then combined and stirred for 1 hour at ambient temperature.

The resulting mixture was transferred into a 100 mL autoclave and heated at 200°C for 24 hours to form the Cu–TiO_2 nanocomposite. After cooling to room temperature, the viscous solution was collected, centrifuged, and washed sequentially with NaOH, ultrapure water, and ethanol multiple times. The obtained nanocomposite was dried at 60°C for 12 hours before characterization.

For comparison, bare TiO_2 nanoparticles were synthesized following the same procedure, excluding the addition of the Cu precursor. Additionally, Cu–TiO_2 samples with varying Cu concentrations (0.5–14 wt%) were prepared and labeled as x% Cu–TiO_2 (x = 1–14).

Characterizations of the prepared catalyst

The prepared photocatalyst analyzed by different characterization techniques. Phase structures of catalyst were examined by (Bruker, D8 Advance) X-ray diffraction. X-ray diffraction (XRD) patterns were captured at 40kV and 40mA via Cu-Kα radiation source (Kα = 1.54056 Å) time 0.1s per dot. Surface charge of the synthesized catalyst is measured by Malvern Zetasizer ZS90 , Malvern potential sample cell (Model ; DTS1070), Temperature -25C, PH 6.5. The morphology and crystal size of the (Cu-TiO_2) photocatalyst were analyzed by Field Emissions Scanning Electron Microscopy (FESEM) Sigma 500, Zeiss, 15kv,30um.Using a UV–Vis spectrometer(UV-3600, Shimadzu, Japan), air as baseline, slit width 5mm, external dual detector, scanning speed medium one point every 0.5 nm. UPS (band edges) analysis carried out by instrumental model "Thermo SCIENTIC ESCALAB 250 Xi'. The X-ray photo-electron spectroscopy used to study the chemical valance state of Cu doped TiO_2 photocatalyst Instrument Model: Thermo SCIENTIFIC ESCALAB 250Xi X-ray Photoelectron Spectrometer (XPS); X-Ray source of radiation: Al Ka source, X-ray energy 1486.6eV, energy resolution better than 0.45eV Tested light spot area of 500 microns, electronic neutralizing gun for charge compensation X-ray tube voltage 15kv, current 10mA, Analytical chamber background vacuum 2* 10-9 mbar. Photoluminescence (PL) emission spectra Fluo time300,PICOQUANTExc_Bandpass 1.5 nm , Exc Polarization 0.0°, Exc Source PDL 820, Exc Filter 1, Exc Intensity 90 %, Exc Attenuation open (5) , Det Band pass 2.7nm, Depolarization, Det Lens Position 7.3mm, Det Attenuation 100 %, Det Filter 400 (4) Det Grating 1200gr 500bl (1), Detector UV-red [PMT], Mean Time 0.1 s, Meas Bin Width 200 ps, Meas Base Resolution 25 ps, Sync Frequency 40000000 , Sync Source PDL 820, Photon Counter Time Harp 260 P 1034100 0121-0422-02.0, Easy Tau 3293, Signal CFD Level -28 mV , Signal CFD Zero Cross -10 mV, Signal Offset -18000 ps, Signal Enable true, Sync CFD Level -150 mV, Sync CFD Zero Cross -10 mV , Sync Offset 0 ps, Sync Div. 8, and Raman spectra (Thermo Scientific DXR3) and Zeta potential also recorded. Surface area and porosity (measured by Micrometrics ASAP 2020 Plus) of the synthesized catalyst were evaluated using N_2 adsorption-desorption measurements. Analysis adsorptive: N2 Analysis bath temp -195.800 °C Thermal correction Yes, Sample mass 0.1225 g, Ambient free space 26.7648 cm^3 Measured Analysis free space 79.5467 cm^3 Equilibration interval 20 s Low pressure dose 8.0000 cm^3/g STP Sample density 1.000 g/cm^3.

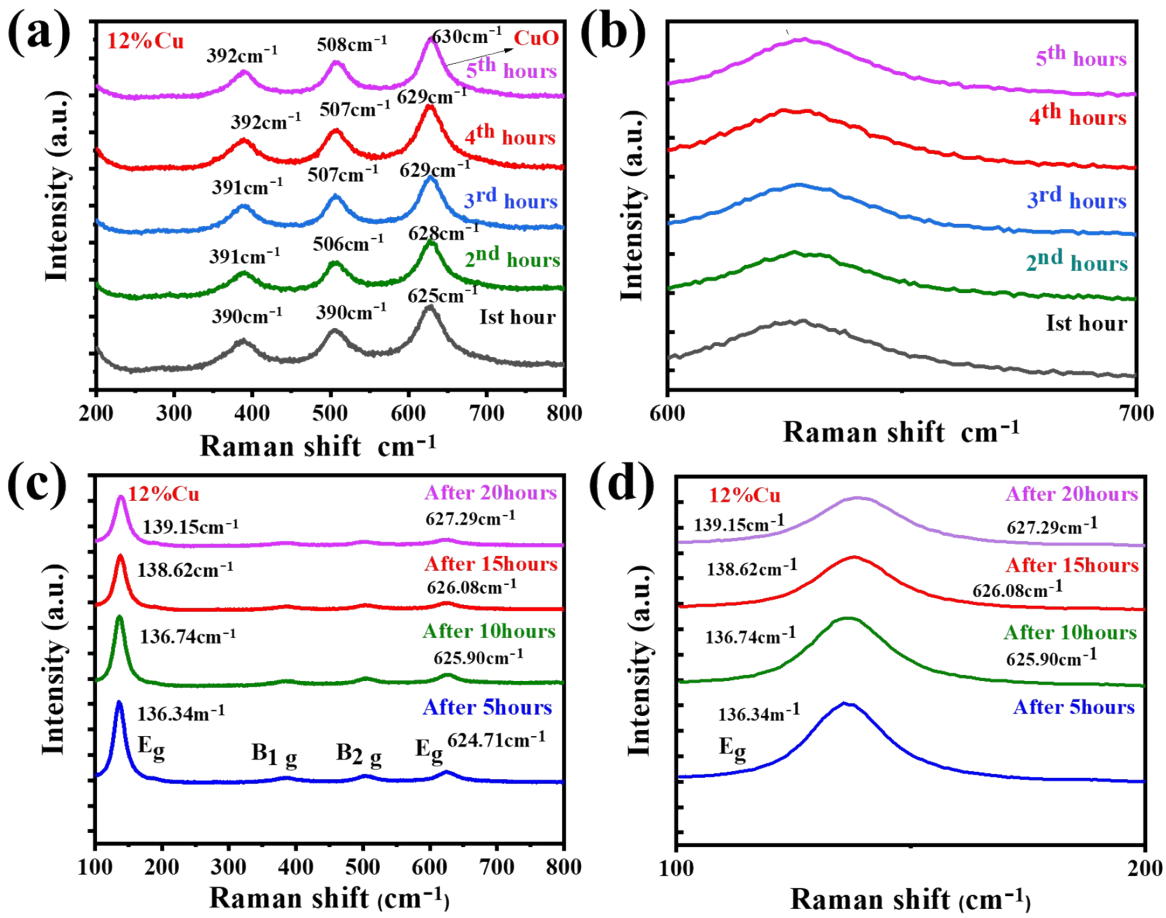

Fig. S2 Raman Shifts of 12% Cu–TiO_2 at different time intervals during HER. **(a)** For one hr. time intervals for 5 hrs. **(b)** Magnified spectra of **a** from 600-700 cm^{-1}. **(c)** At 5 hrs. time interval during 20 hrs. of HER. **(d)** Magnified spectra of **c** from 100-200 cm^{-1}.

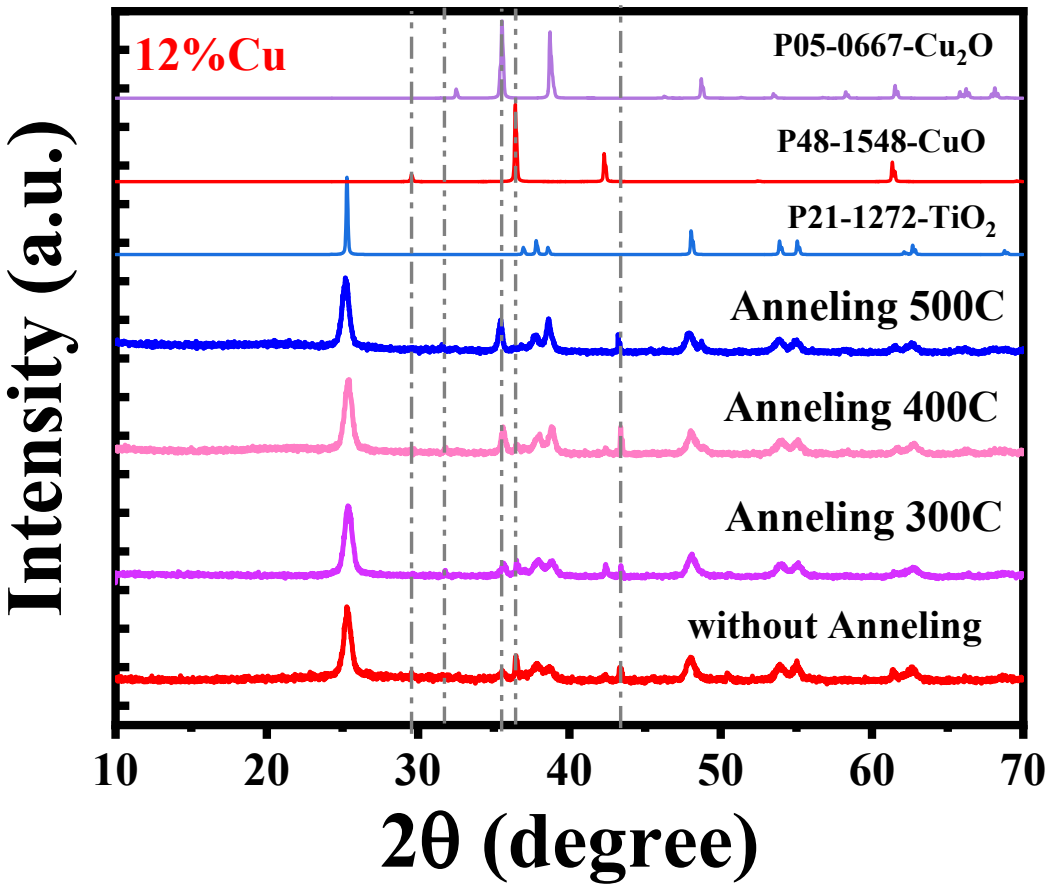

Fig. S3 XRD Sepectrum of 12%Cu-TiO_2 after anealing at different temperature. Conversion of CuO to Cu_2O is evident.

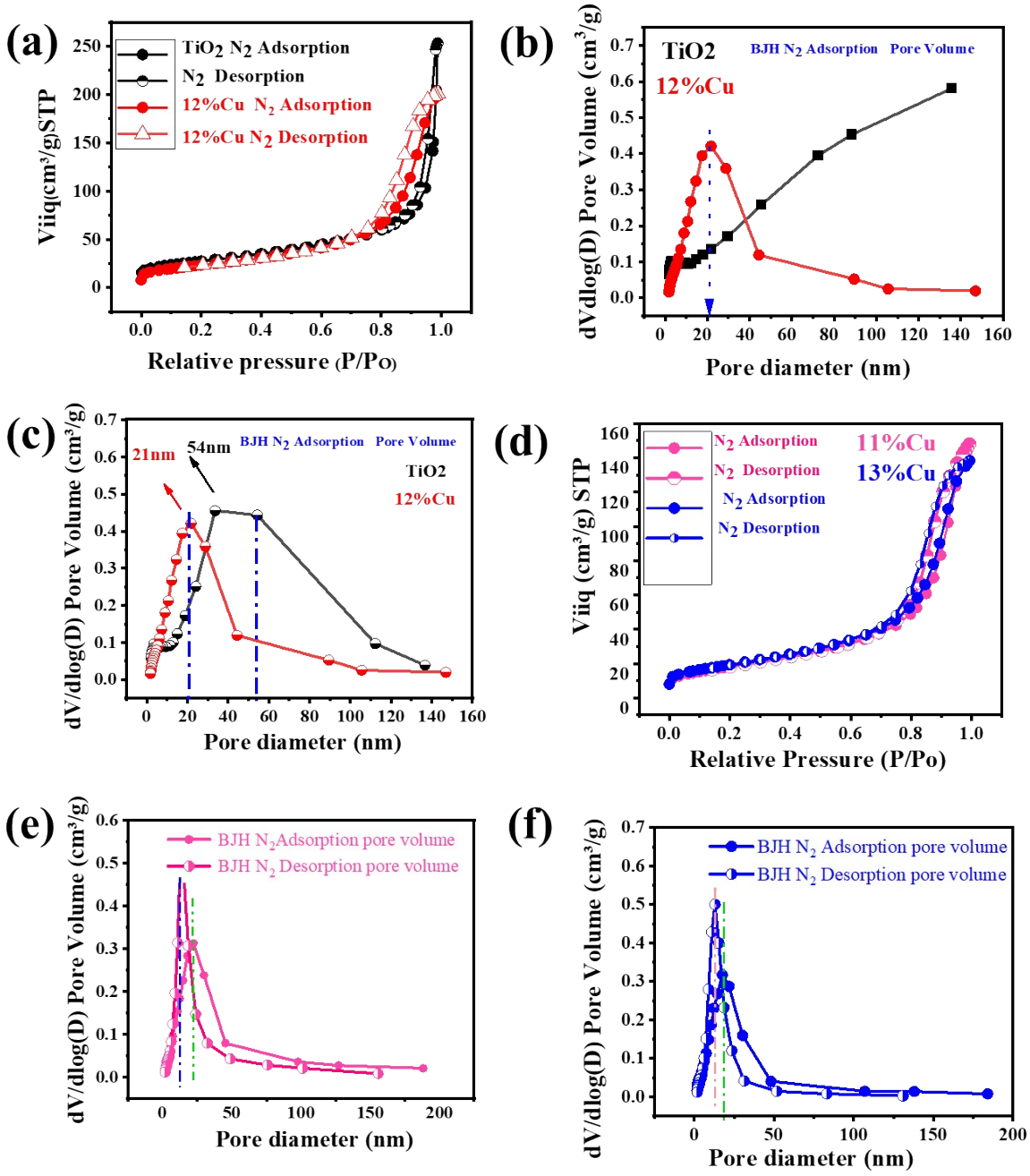

Fig. S4 (a) N_2 adsorption & desorption of 12 % Cu–TiO_2 **(b-c)** BJH adsorption & desorption pore size distribution of 12%Cu-TiO_2 **(d)** N_2 adsorption & desorption of 11 & 13 % Cu–TiO_2 **(d-f)** BJH adsorption & desorption pore size distribution of 11 and 13 %Cu-TiO_2

Table.S1 BET and Band gap Analysis.

No	Synthesized Catalyst	BET surface Area (m2/g)	Pore Volume (cm^3/g)	Average pore size (nm)	Band gap Energy (eV)
1	TiO_2	97.0	0.39	16.1	3.0
2	11%Cu	65.9251	0.23	13.8964 nm	2.3
3	12%Cu	83.9	0.31	14.7	2.1
4	13%Cu	70.03	0.214003	12.2228	2.0
5	14%Cu	-	-	-	1.7

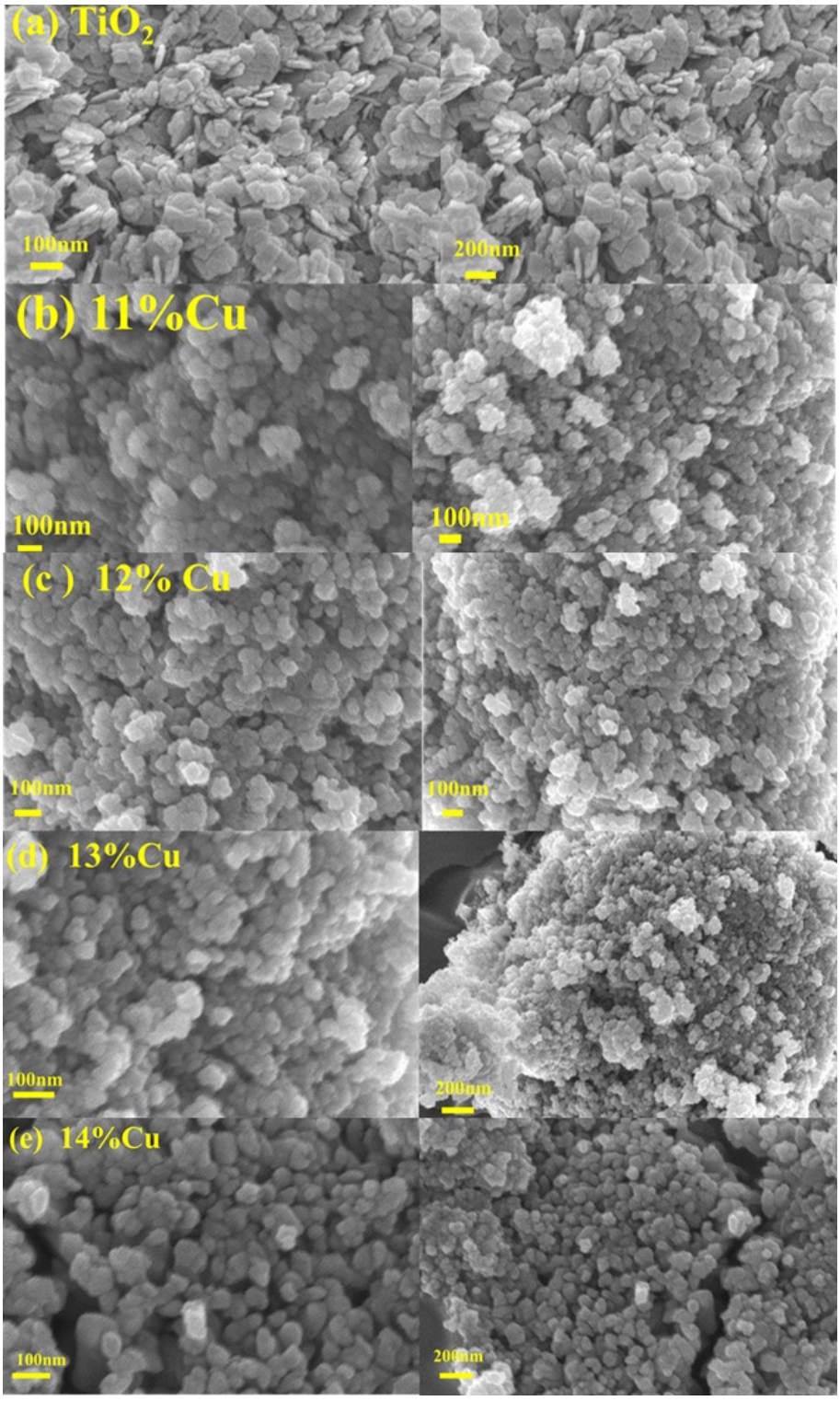

Fig. S5 (a) SEM images of pristine TiO_2 and **(b-e)** different Cu doped TiO_2 (11-14% Cu) samples.

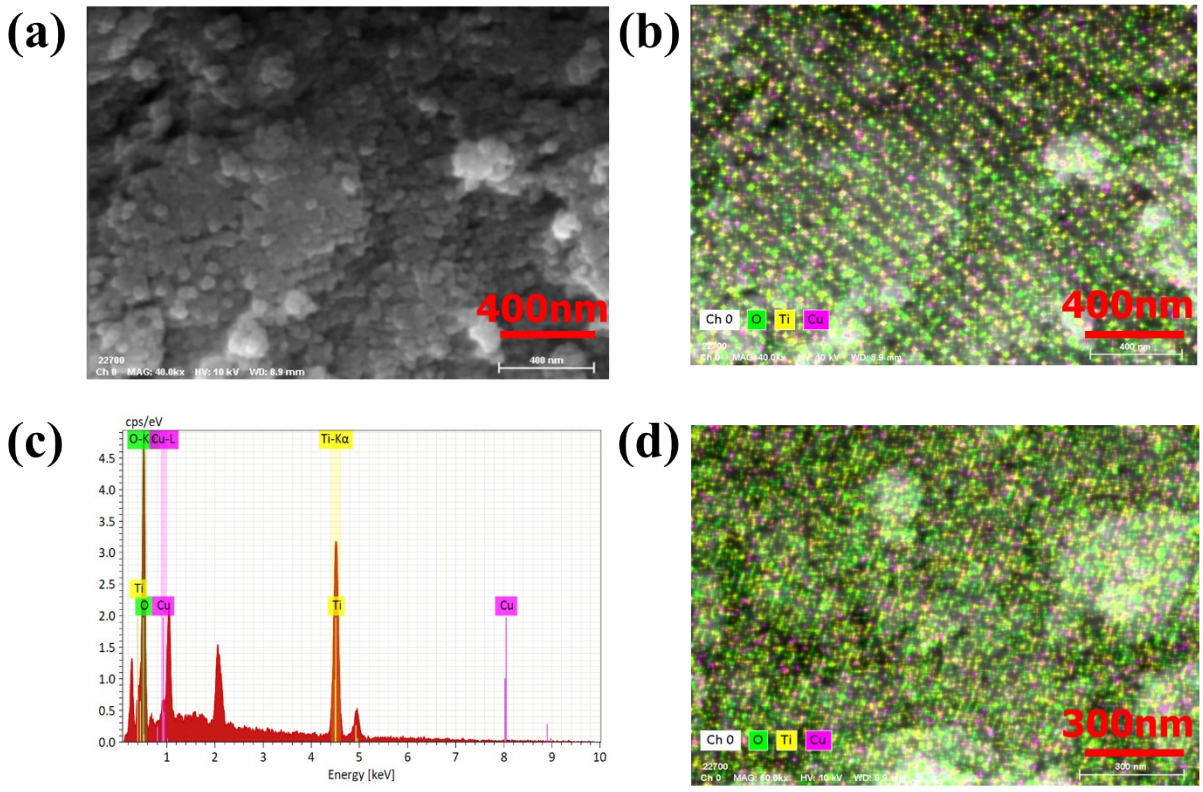

Fig. S6 (a) EDS mapping of 12%Cu, shows complete dispersion of Cu over TiO_2 (**b, d)** EDS line scanning of 12%Cu **(c)** Selected region for EDS mapping of 12%Cu.

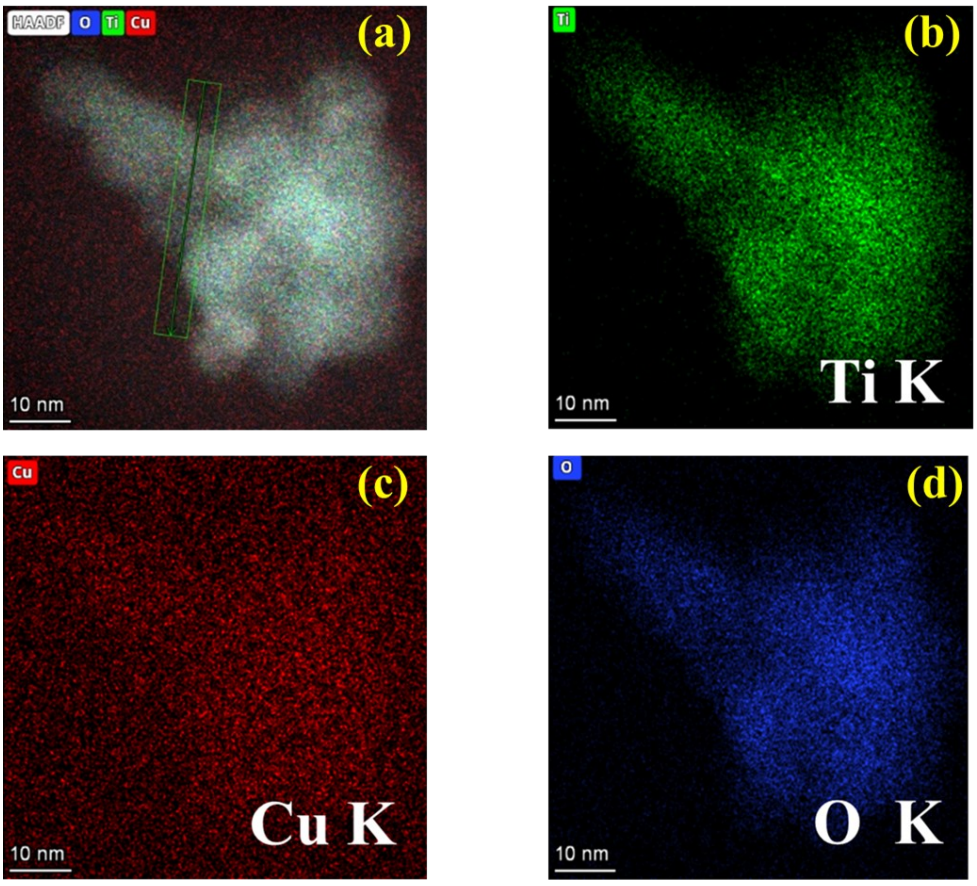

(e)

Z	Element	Family	Atomic Fraction (%)
8	O	K	67.12
22	Ti	K	22.95
29	Cu	K	9.92

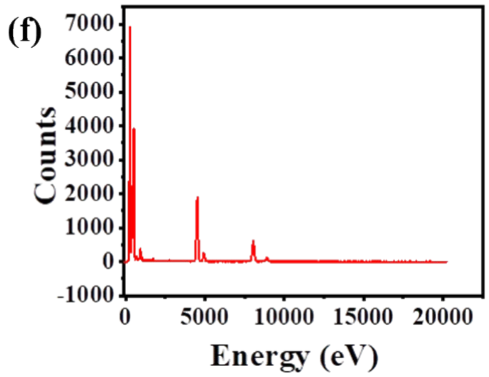

Fig. S7 (a-f) The high angle annular dark-field scanning transmission electron microscopy (HAADF- EDS) line scan of Cu, Ti, and O of 12%Cu.

Table. S2 Comparison of high H_2 production with Cu-doped TiO_2 catalyst.

No.	Photocatalyst	Preparation Method	Light condition	Sacrificial reagent 20%CH_3OH/water	HER rate (mmol $g^{-1}h^{-1}$)	Year/Ref.
1	CuO-TiO_2(P25)	Multistep Hydrothermal method	UV-excitation	80%EtOH	20.3	2013[1]
2	3%Cu_2O-TiO_2	Impregnated copper	125W Hg lamp	10%CH_3OH	18	2014[2]
3	Cu_2O-TiO_2	Multistep solvothermal & Photo deposition process	300 Xe lamp	10%CH_3OH	32.6	2019 [3]
4	0.75%CuSA/TiO_2	Multistep hydrothermal	UV	25%CH3OH	16.6	2019[4]
5	Cu_2O-TiO_2 ($H_2Ti_3O_7$)	Two-step Solvothermal Process	300 W Xe lamp	10%CH_3OH	24.83	2019[5]
6	1 % Cu/TiO_2(P25)	Multistep Sol-gel	UV lamp	20% CH3OH	15	2020[6]
7	3%Cu -TiO_2 (Nano sheet)	Multistep Impregnation method	300 W Xe lamp	20%CH_3OH	18	2021[7] **Previous work**
8	0.4%Cu-TiO2	Multistep Sol-gel	300 W Xe lamp	MeOH	21	2022[8]
9	1%Cu-TiO_2/500	One pot Hydrothermal Method	UV-Vis LED	CH_3CH_2OH	20.2	2023 [9]
10	Cu-TiO_2/$SrTiO_3$	Multi-step sol-gel	UV lamp	10% CH3OH	13.62	2023[10]
11	Cu_2O-TiO_2(P25)	Hydroxylation Process	300 W Xe lamp	25%MeOH	15	2023[11]
12	Cu/Pr-TiO2	Multistep Hydrothermal	UV LED	25% MeOH	32.88	2024[12]
13	12%CuO_x-TiO_2	One-pot Hydrothermal Synthesis	300 W Xe lamp	20%CH_3OH	30.6	**This work**
14	13%CuO_x-TiO_2	One-pot Hydrothermal Synthesis	300 W Xe lamp	20%CH_3OH	17.18	**This work**
15	CuO-TNT	hydrothermal	400 W high pressure Hg lamp	10 % methanol	64.2-71.6 mmol h^{-1} g^{-1}	2011[13]
16	Cu_2O/TiO_2	alcohol-thermal method	(300 W Xenon lamp)	methanol	24.84mmol/g	2022[14]
17	CuxO/TiO_2	wet impregnation	(300 W Xenon lamp)	methanol	6mmol/g/h	2011[15]
18	Cu/TiO2	incipient wetness technique.	A xenon arc lamp (Oriel Model No: 6271)	methanol	0.2mmol/g/h	2021[16]
19	$Cu_{0.02}Ti_{0.98}O_{2-\delta}$	Sol-gel method	p (Hg, Ace Glass Inc., 450W)	methanol	333micromol /g/h	2016[17]
20	10CuGT	Wet impregnation	(300 W Xenon lamp)	methanol	10mL/h	2009[18]

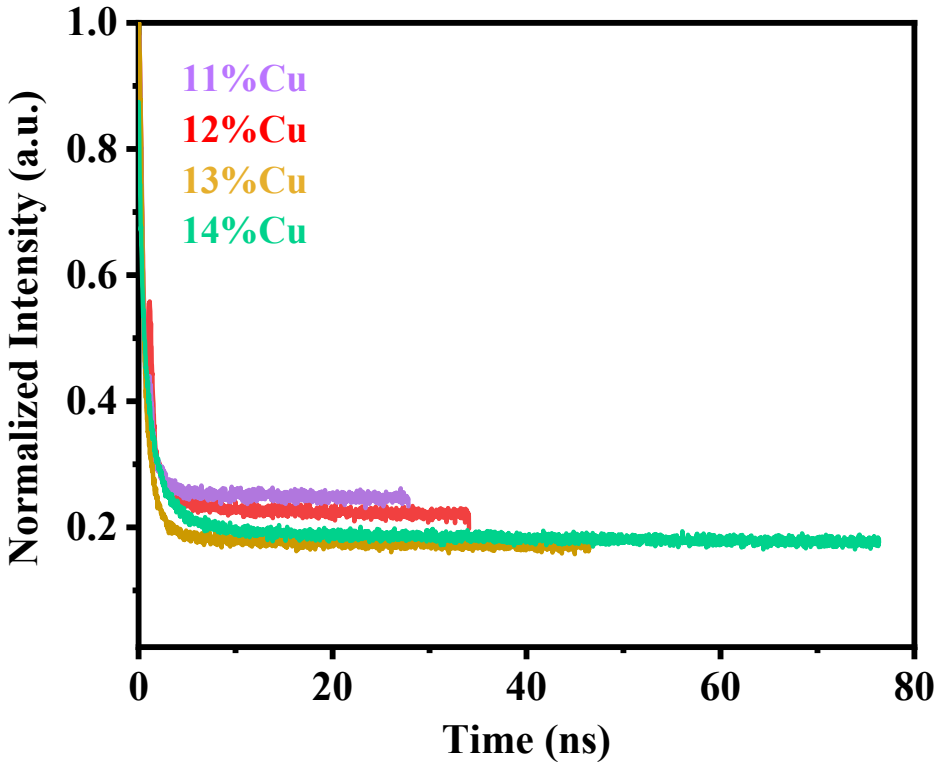

Fig. S8 Time Resolve photoluminisence (TRPL) of pristine TiO_2 and 11-14 %Cu-TiO_2 catalyst.

Table S3: Time decay of different wt% Cu.

Prepared catalyst	**Time decay(ns)**
TiO_2	3.221
11% Cu	2.34
12% Cu	0.796
13% Cu	3.341
14% Cu	2.96

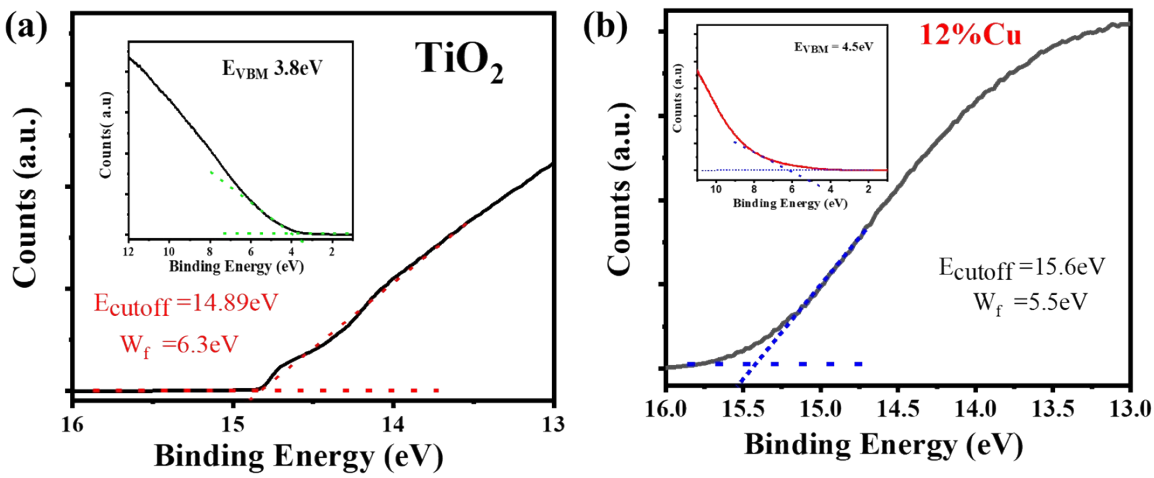

Fig. S9. UPS analysis (Band edges) of TiO_2 (**a**) and 12%Cu (**b**).

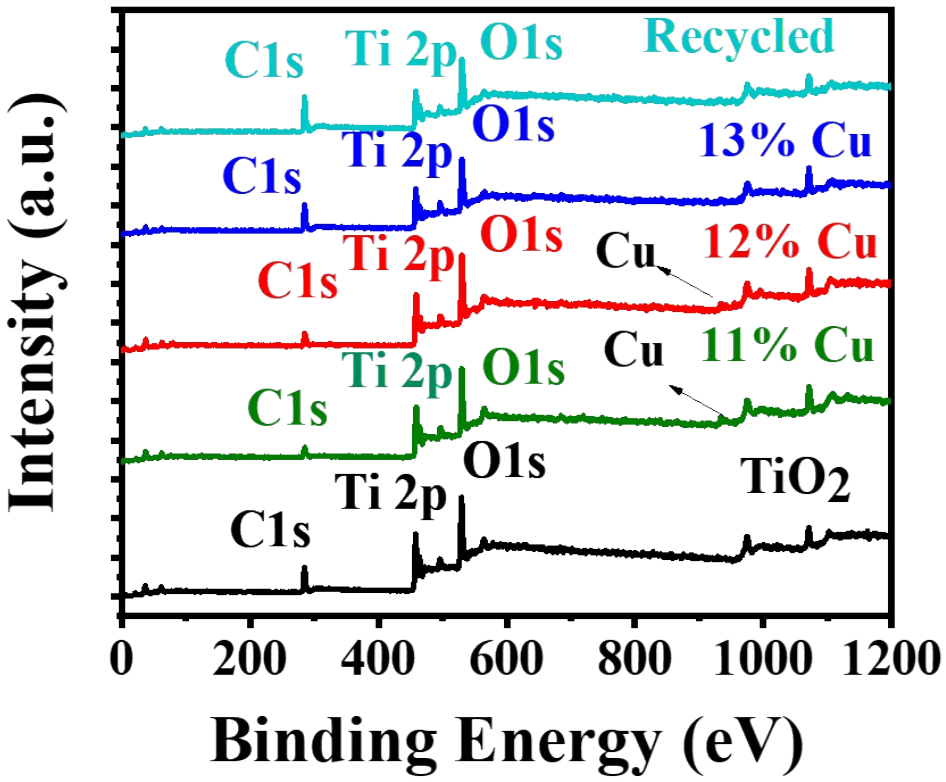

Fig. S10 (a) XPS full survey scan of TiO_2 and %Cu-doped TiO_2.

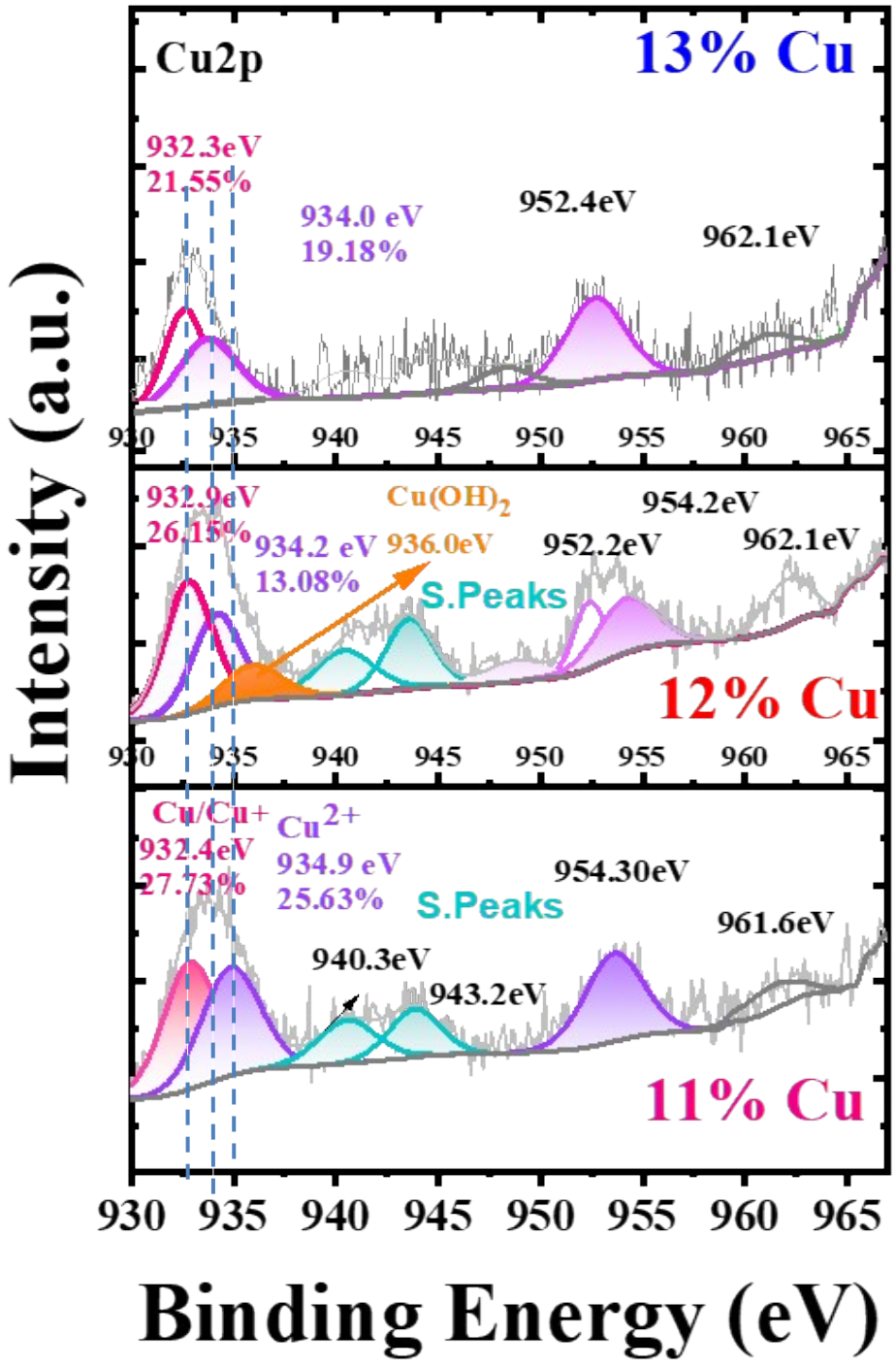

Fig. S10 (b1) Cu2p scan of 11-13%Cu−TiO_2. A comparison of Cu $2p_{3/2}$ spin-orbit peak intensities reveals the composition ratio Cu^0/Cu^+ : Cu^{2+} (~1:1 for 11%Cu−TiO_2) increases with doping, reaching a maximum (~2:1 for 12%Cu−TiO_2). The highest insensity of satellite peaks around 940 eV and 944 eV, typical characteristics of CuO, implying the maximum doping for 12%

$Cu-TiO_2$. The approximated concentration trend at surface found to be: $CuO>Cu>Cu_2O$ ($11\%Cu-TiO_2$), $Cu_2O>Cu>CuO$ ($12\%\ Cu-TiO_2$), and $Cu>Cu_2O>CuO$ ($13\%Cu-TiO_2$), which is consistent with XRD results.

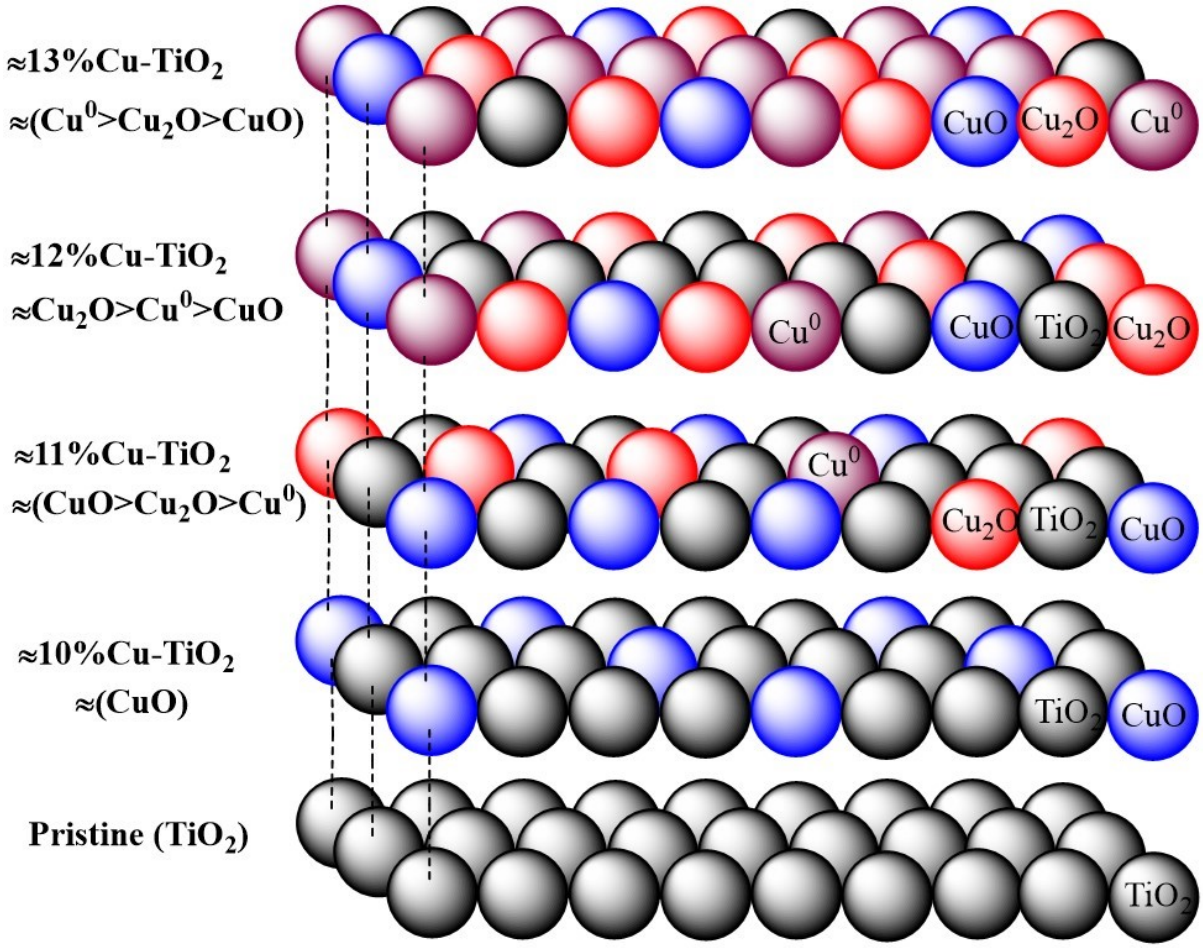

Figure 10b2. Sketch showing proposed %Cu doped TiO_2 at surface.

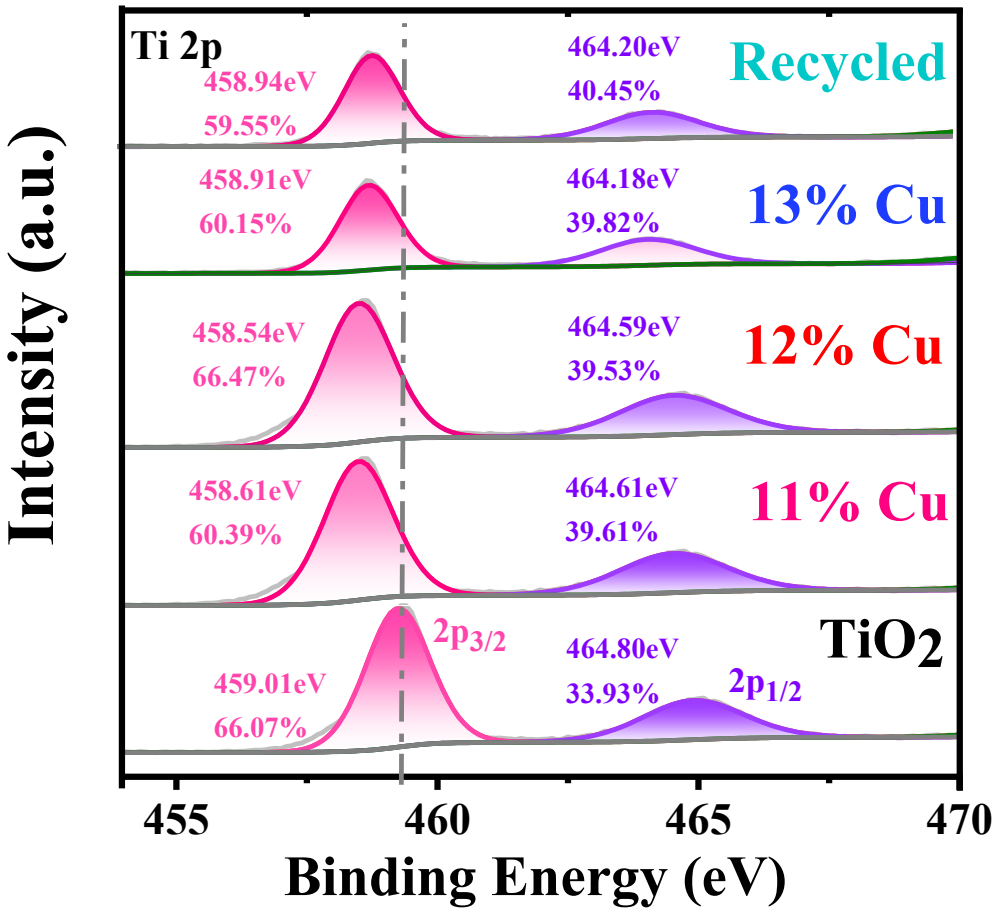

Fig. S10 (c) Ti2p scan of 11% Cu, 12% Cu, 13% Cu, and recycled (12%).

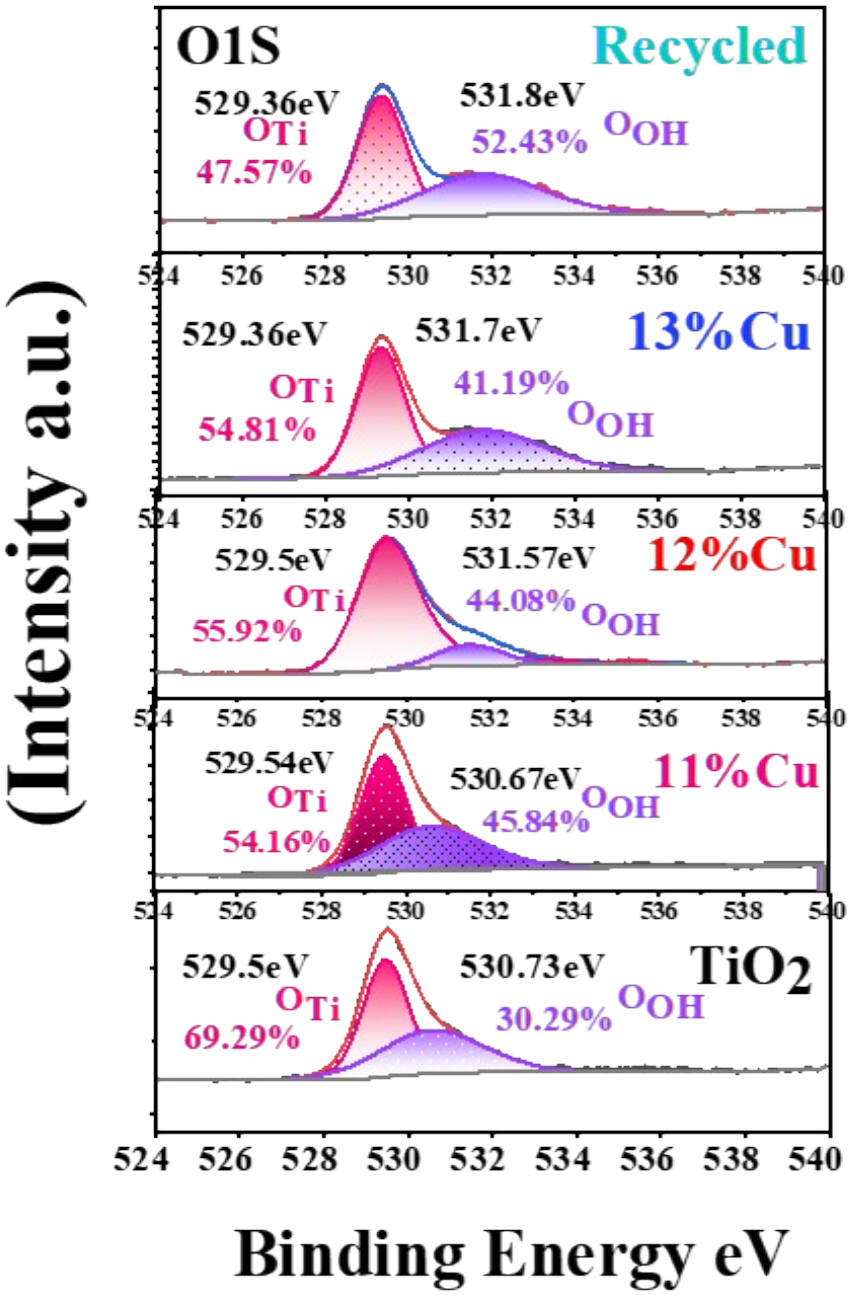

Fig. S10 (d) O1S Scan of pristine TiO_2 and %Cu doped TiO_2.. Compared to pristine TiO_2, in 12%Cu−TiO_2, the OH peak intensity increasing from ~30% to 44%, indicating an increase in available OH adsorption sites. The binding energy difference (ΔE_{BE}) between Ov and OH widen from 1.5 eV in pristine TiO_2 to 2.44 eV (11%), 2.56 eV (12%), and 2.55 eV (13%) in CuOx−TiO_2.

S11. Photo -catalytic reaction experimental details

The photothermal water-splitting test was conducted at room temperature using an airtight 200 mL quartz reactor. The reactor's inlet and outlet were sealed with silicone rubber sockets to prevent product leakage. A total of 0.02 g (20 mg) of photocatalyst powder was dispersed in 100 mL of a water-methanol solution (80 mL water, 20 mL methanol, 4:1 ratio) and ultrasonically treated for 20 minutes to achieve a homogeneous dispersion.

Before light irradiation, the reaction system was purged with high-purity N_2 for 6 minutes to eliminate oxygen and create an inert environment within the reactor. The photocatalytic reaction was carried out under a focused Xe arc lamp (Au Light, China). Throughout the experiment, the solution was continuously stirred magnetically to maintain homogeneity.

After one hour, the produced H_2 gas was collected and analyzed using an offline gas chromatograph (GC-2018, Shimadzu, Japan) equipped with a thermal conductivity detector and a molecular sieve 5A column, with N_2 as the carrier gas. To evaluate recyclability and reproducibility, the produced H_2 from the 12% Cu-TiO_2 sample was removed at regular 5-hour intervals and replaced with N_2 for the next cycle. The H_2 evolution process was repeated for 20 hours (four cycles).

The results, shown in Figure 7(b), indicate a 95% H_2 production retention after four cycles (20 hours), demonstrating excellent catalytic stability and high resistance to photo corrosion.

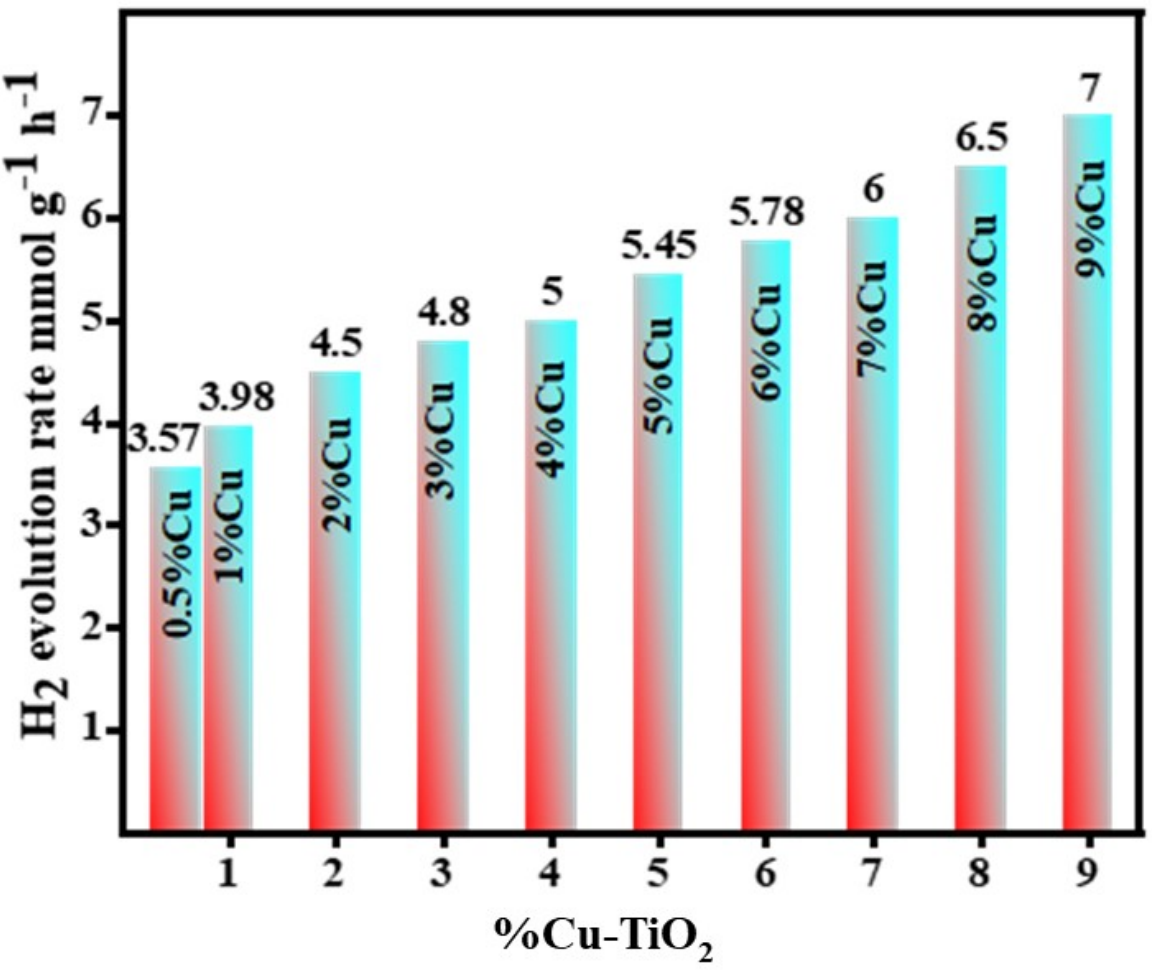

Fig. S12 Hydrogen evolution rate in mmol·g^{-1}·h^{-1} at different %Cu-TiO_2.

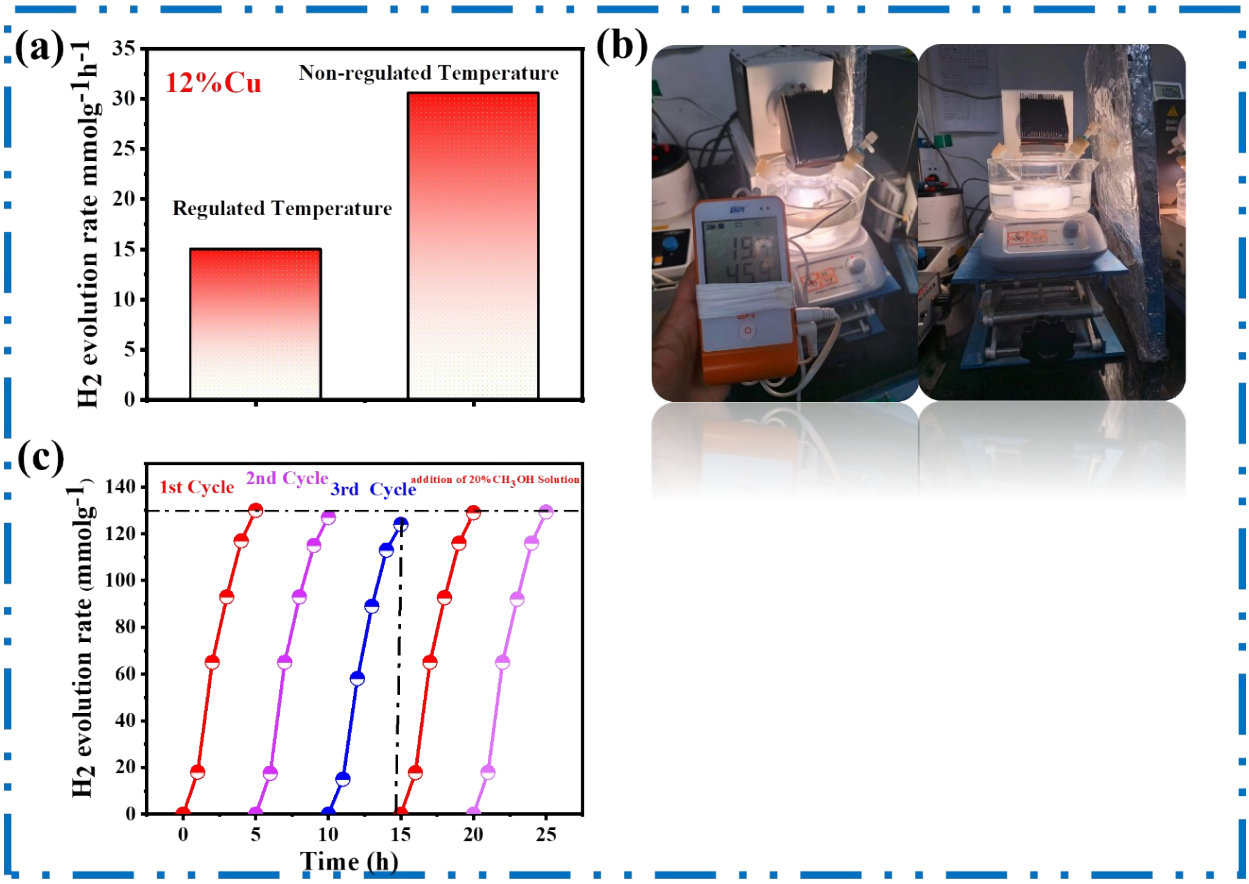

Fig. S13 (a-b) Water bath temperature regulated H_2 evolution tests of 12%Cu-TiO_2 at 20 ^{0}C vs non-regulated temperature (40-45 ^{0}C). **(c)** 100% recovery of HER was observed after replenishment of 20% methanol following 15 h of operation.

S14. Apparent Quantum Yield

The apparent quantum efficiency (AQY) of $12\%Cu$ is calculated via the following formula:

$$AQY(\%) = Ne/Np$$

Ne is the total number of electrons transferred during reactions, Np is the number of incident photons, and n represents the number of evolved hydrogen molecules. The calculation formulas are given as:

$Ne = 2 \times \frac{n}{Np}$,

$$Np = IA\lambda.\frac{t}{hc}.$$

Where I is the incident photons, A is the incident light area, t is the reaction time, λ represents the incident light wavelength, h is Planck's constant, and c is the speed of light. The average power of UV light $(416 + 10nm)$ is $52.76mW/cm^2$, which was identified by a photo-radiometer $(PL - MW\ 2000,$ Perfect Light$)$. The highest hydrogen production rate of $0.82mmol$ in two hours for the $12\%CuO - TiO_2$ was used to calculate t, so the value of Ne was estimated to be 8.66×10^{20}. The diameter of the photocatalytic reactor is $5.5cm$, so the value of A should be $23.5cm^2$, the reaction time t is $3600sec$, and the AQE of $12\%CuO - TiO_2$ irradiated by $416nm$ light is 49.2%, by substituting the above value into the given formula. AQE at $416nm$ is 9.28%. Calculation steps are as follows.

$AQE(\%) = (Ne/Np)100\%$

$$AQE(\%) = (8.669 \times 10^{20}/9.335 \times 10^{21})100\%$$

$$AQE(\%) = 9.28\%.$$

Now for the same set of values $(I = 52.76 \times 10^{-3}W\backslash cm^2,\ A = 23.5cm^2,\ t = 3600sec)$ except when the highest H_2 production rate of $0.673mmol$ in 2 hours are used. Then $Ne = 8.669 \times 10^{20}$ and at $450nm$ the corresponding AQE is 9.782%.

S15. Computational Details

All the calculations were performed using the Vienna Ab initio Simulation Package (VASP version 5.3.5)[14, 15] employing periodic density functional theory (DFT). The projected augmented wave (PAW) pseudopotentials determined the interaction between core and valence electrons.[16] The generalized gradient approximation's (GGA) PBE functional was utilized to account for the exchange-correlation interactions.[17, 18]

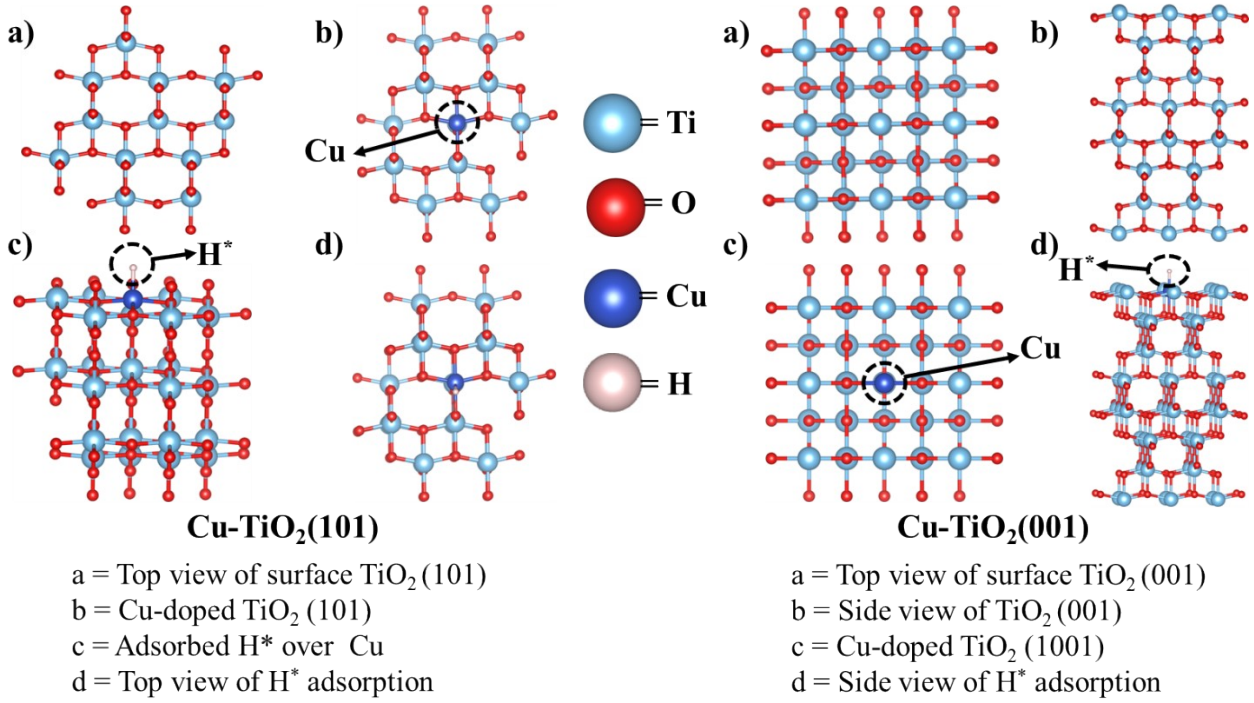

Fig. S15. Optimized Cu doped anatase TiO_2 supercell for (101) and (001) phases and showing H* adsorption.

The van der Waals interaction was computed using Grimme's semi empirical dispersion-corrected DFT-D3 technique. For the plane-wave expansion, 400 eV was chosen as the cut-off energy. The unit cell consists of Ti and O atoms using a 2× 2× 1 supercell of TiO_2. In a cubic unit cell, the interlayer distance of 15 Å was used to avoid the interaction between the layers. To get the desired level of accuracy, a 1× 1× 1 K-sampling point was used for the Brillouin zone grid sampling. The geometry optimization was carried out at a convergence level of 10^{-5} eV and atoms were allowed to relax until the optimum force was<0.02eVÅ^{-1}. The AIMD simulations were carried out within the Canonical (NVT) ensemble, emphasizing temperature-dependent features at constant temperature, particle number, and volume. The temperature was

regulated using a Nosé-Hoover thermostat, which is optimal for sustaining a uniform thermal environment during the simulations with SMASS=0 at the Nosé-Hoover thermostat (MDALGO = 2).

In this section, we present the optimized atomic structures of Cu-doped anatase TiO_2 surfaces for the (101) and (001) facets, as shown in **Fig.S15**. Both surfaces were modeled using slab models with a vacuum layer of approximately 15 Å along the z-direction to avoid the interlayer interactions.

For the TiO_2 (101) and TiO_2 (001) surfaces:

- The slabs were constructed from optimized bulk anatase TiO_2, cleaved along the respective crystallographic planes using material-studio package. The lattice parameters used for 001 phases are (a = b = 7.552Å, c = 31.6005Å) and for 101 are (a = 10.88Å b = 7.552Å, c = 27.42Å)
- The (101) surface model consists of a 4 × 2 supercell with four atomic layers, whereas the (001) surface model uses a 3 × 3 supercell with five atomic layers.
- During structural relaxation, the bottom two layers were fixed to simulate bulk-like behavior, while the remaining layers and adsorbates were fully relaxed.

Cu Doping Strategy: We achieved by substituting a surface Ti atom with a Cu atom, simulating the substitutional doping mechanism. This substitution is energetically favorable and allows the Cu dopant to directly interact with the surface-adsorbed species.

Hydrogen adsorption model (H^*): After Cu-doped model by placing a single hydrogen atom (representing a proton-electron pair) over the Cu site towards estimating the final adsorption energies. The initial adsorption configurations were carefully chosen on taking the entropy (ΔTS) and zero-point energy difference (ΔZPE) of 0.24 eV.

- In TiO_2–Cu–(101), the H^* was preferentially adsorbed at top of cupper atom adjacent to the oxygen atom.
- In TiO_2–Cu–(001), the H^* also favored adsorption near surface cupper atoms neighboring the oxygen atom.

Throughout the relaxation process:

- All atomic forces were converged below 0.02 eV/Å.
- A plane-wave cutoff energy of 400 eV was employed at DFT-D3 method using
- Monkhorst–Pack k-point grids of 1×1×1 was used for Brillouin zone sampling.

Structural Analysis:

After Cu doping:

- Significant relaxation is observed around the Cu site due to its lower oxidation state compared to Ti^{4+} and its larger atomic radius.

- The Cu atom slightly protrudes from the surface plane, particularly noticeable in the (001) surface configuration.
- Upon H^* adsorption, local distortions are further enhanced, indicating strong H^* binding facilitated by the modified electronic structure of Cu sites.

The optimized structures (top view and side view) in **Fig.S15** demonstrate that Cu doping introduces localized distortions at the surface due to the different ionic radius and electronic structure of Cu compared to Ti. The adsorption of H^* leads to further local relaxation, particularly around the Cu and adjacent O sites, indicating strong interactions that could enhance hydrogen evolution reaction (HER) activity. The high catalytic activity of the 101 phase is supported by electronic descriptors as described in the main manuscript. We added the charge transfer analysis for both phases using the grid-based Bader charge (q) and found that the highest charge transfer was observed for the phase (101) at 1.41eV and 0.71 eV for the (001) phase. Later this elucidated by finding the charge density differences as depicted in **Fig.8 (c)** in the revised main manuscript.

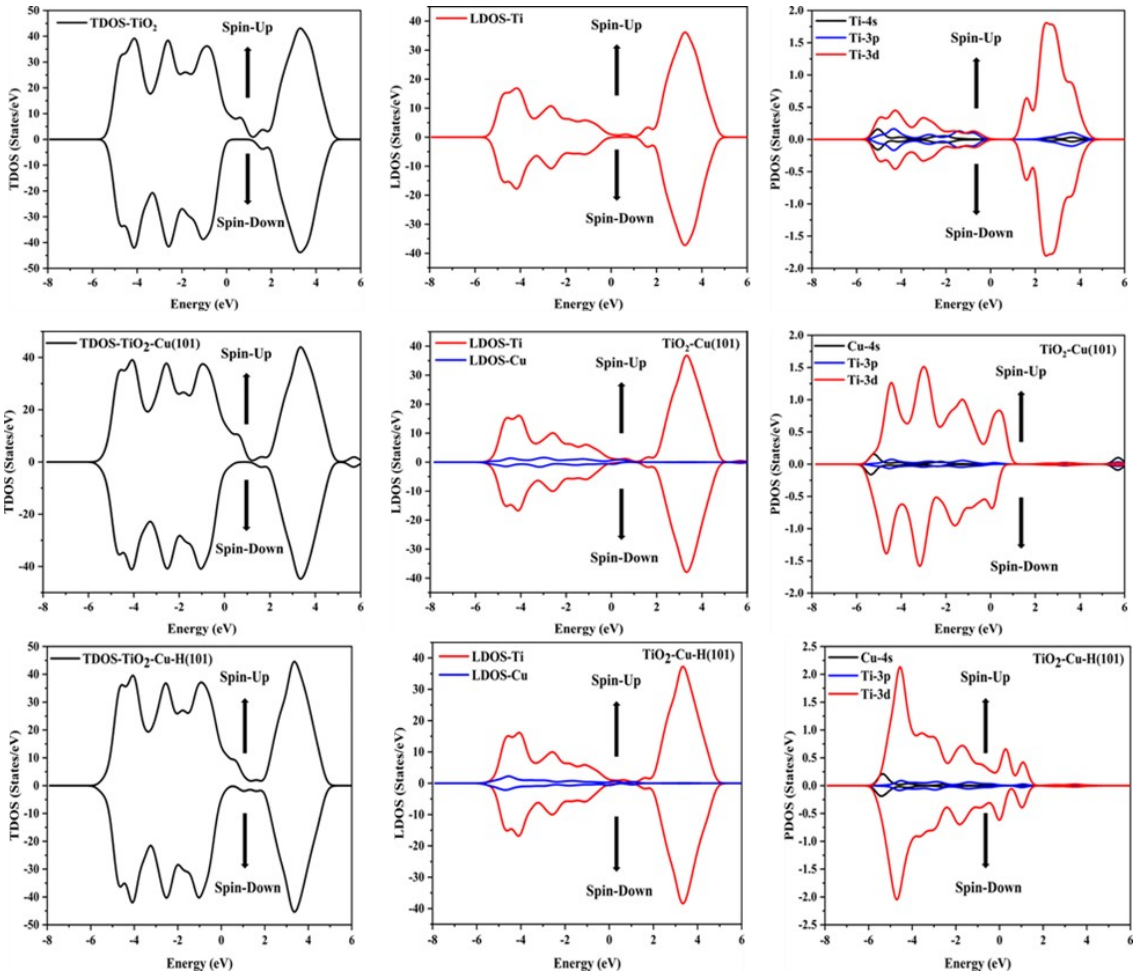

Fig. S16 The density of state analysis using Total density of state (TDOS), local density of state (LDOS), and Projected density of state (PDOS) for the TiO_2 surface, Cu-doped TiO_2 at 101 phases with and without hydrogen adsorption.

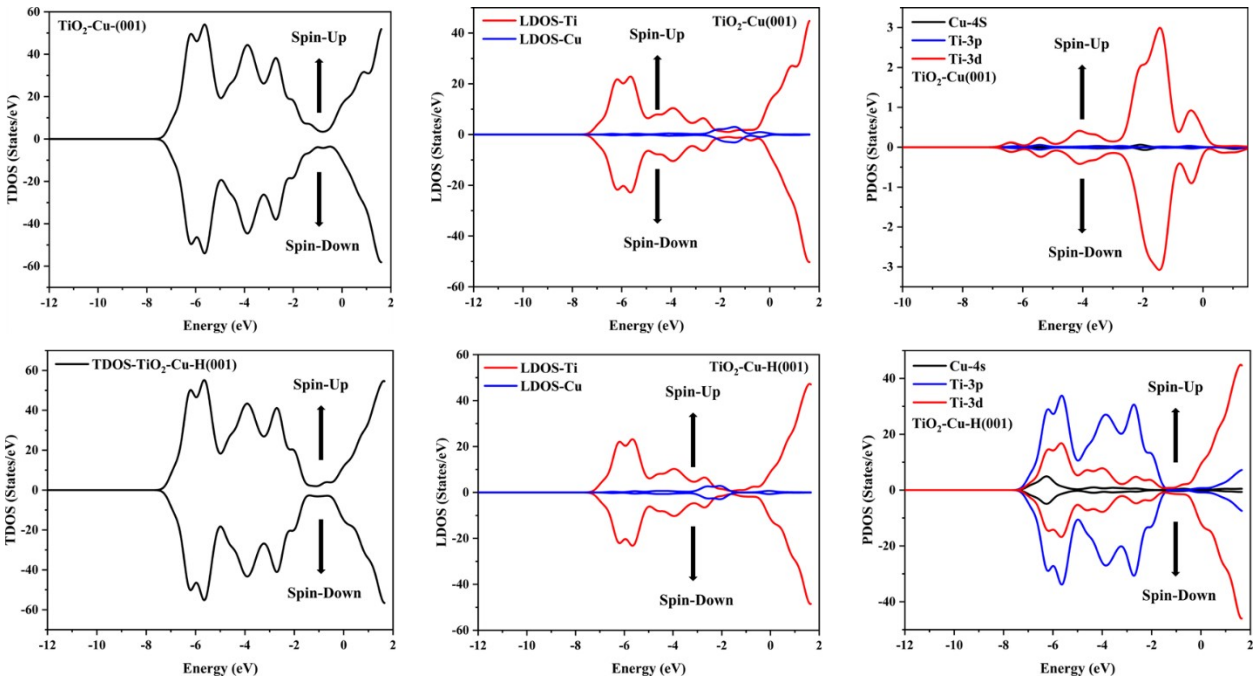

Fig. S17 The density of state analysis using Total density of state (TDOS), local density of state (LDOS), and Projected density of state (PDOS) of Cu-doped TiO_2 at 001 phase with and without hydrogen adsorption. Phase 001, depicts the greater contribution shown by Ti orbitals in LDOS for both with and without hydrogen atoms. While examining the PDOS, d-orbitals contribution becomes more prominent, on adsorption of hydrogen atom over the TiO_2-Cu-001 surface, Ti-3p orbitals show the major contribution as compared to Ti-3d orbitals due to undesired orbitals contribution making it unsuitable candidate for HER.

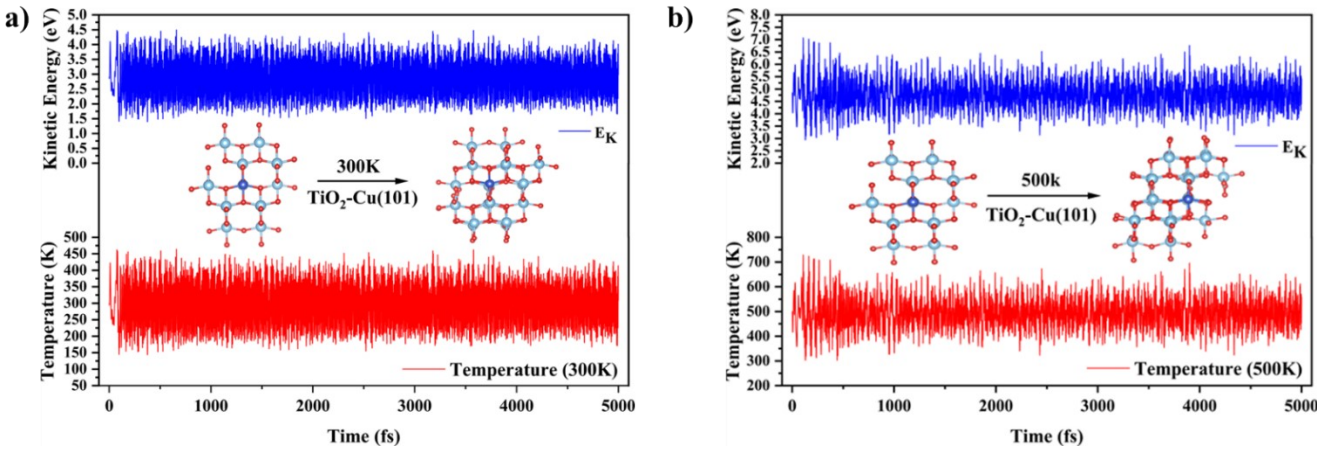

Fig. S18 (a-b) The AIMD plots of the best catalyst at 300k and 500k by plotting temperature and kinetic energy trend at 5000 ionic steps (fs) using the same level of theory.

Table. S4 Gibbs free energy (ΔG_{H^*})

The optimization energy, difference of zero-point energies (ZPE), and entropy (TΔS) of the system are calculated at temperature (298.15K) and pressure 1 atm. The hydrogen adsorption energies (ΔE_{H^*}) are also calculated for both phases. The lowest Gibbs free energy (ΔG_{H^*}) is depicted by phase (101). All the energies are measured in (eV).

Molecules	opt-energy	(ΔZPE-TΔS)	Supercell size	ΔE_{H^*} (eV)	ΔG_{H^*} (eV)
TiO_2 (101)	-656.57	---	2*2*1	---	---
Cu−TiO_2(101)	-643.11	---	-	---	---
Cu−H−TiO_2(101)	-646.91	0.28	-	-3.79	-0.06

TiO_2 (001)	-786.89	---	-	---	---
Cu−TiO_2 (001)	-779.88	---	-	---	---
Cu−H−TiO_2 (001)	-784.17	0.17	-	-4.28	-0.65

Table. S5 Theoretically calculated charge and bands energy values in eV

The theoretically calculated Bader charge (q), s-band center, p-band center, and d-band center (εd) of pure

TiO_2 surface and doped cu surface at two different phases (101) and (001). The work function (WF) and Vacuum level (VL) are also used to determine how much energy is required to transport an electron to vacuum outside the solid surface. All the parameters are measured in units (eV).

The value of the single doped metal atom over the TiO_2 at phase 101 and 001 d-band center value may be determined using the provided equation.[19]

$$\varepsilon d = \frac{\int_{-\infty}^{\infty} n_d(\varepsilon)\varepsilon d\varepsilon}{\int_{-\infty}^{\infty} n_d(\varepsilon) d\varepsilon} \qquad \textbf{(Eq. S2)}$$

The "n_d" symbol represents the d states of individual metal atoms. The d-band center of metals atoms is

Molecules	**Bader Charge (eV)**	**s-band center (eV)**	**p-band center(eV)**	**d-band center (eV)**	**WF (eV)**	**VL (eV)**
TiO_2 (101)	2.6	6.58	1.93	0.91	9.132	4.668
Cu-TiO_2(101)	1.41	6.42	1.87	0.81	9.143	4.622
Cu-TiO_2(001)	0.71	4.05	3.76	1.91	2.841	3.339

crucial to investigate the catalytic activity, can be determined using Eq. S2.

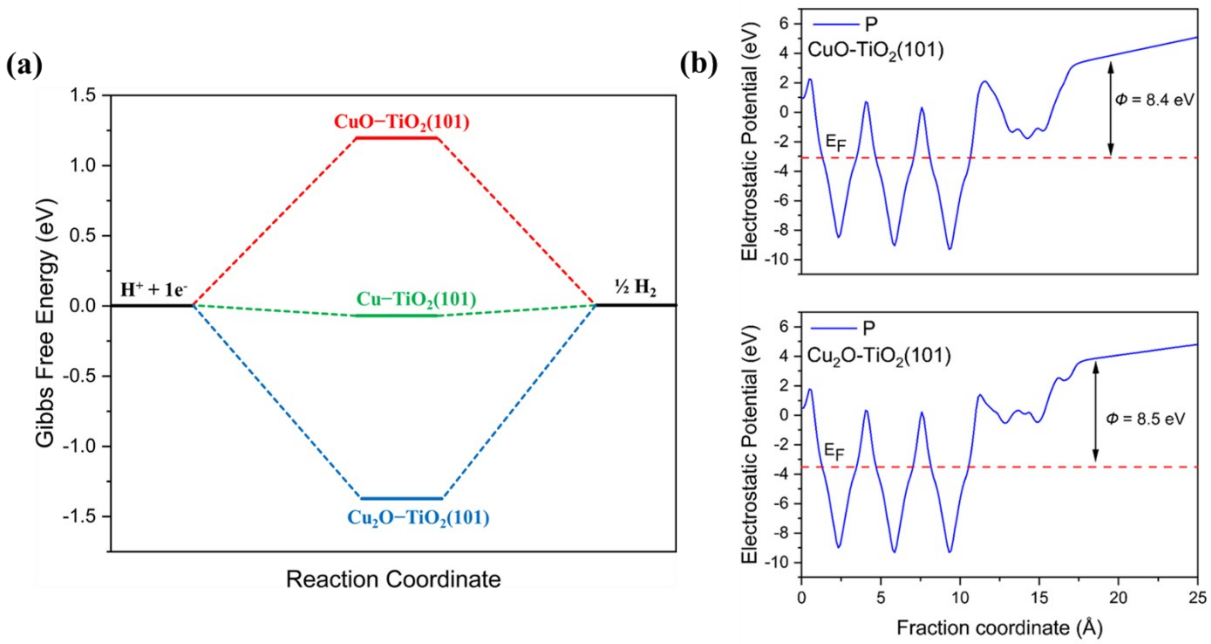

Fig. S19 (a) Gibbs free energy profile of Cu−TiO_2(101), CuO−TiO_2(101), and Cu_2O-TiO_2(101) **(b)** The DFT computed work function (Φ) values of the CO−TiO_2(101), CuO−TiO_2(101), and Cu_2O-TiO_2(101).

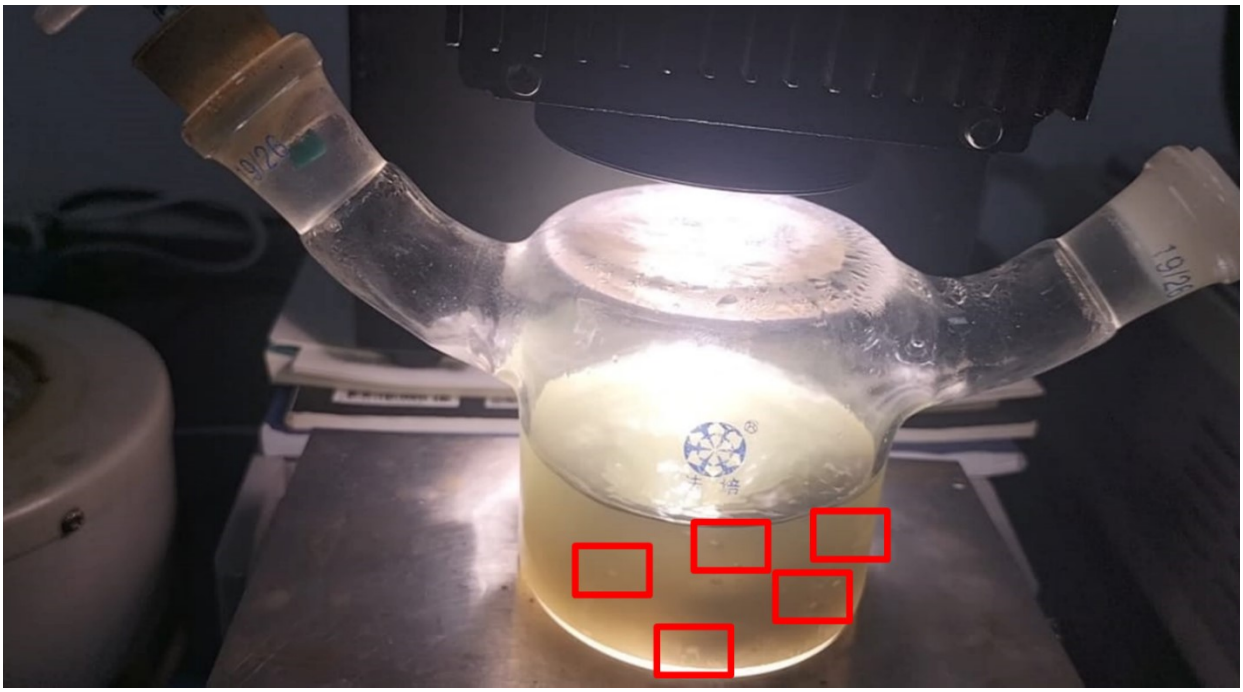

Fig. S20 Photoshoot of hydrogen bubbles marked with red rectangle during HER-test under xenon lamp at room temperature.

References

1. Wan-Ting, C., et al., *The role of CuO in promoting photocatalytic hydrogen production over TiO2.* International Journal of Hydrogen Energy, 2013. **38**(35): p. 15036–15048.
2. Valero, J.M., S. Obregón, and G. Colón, *Active site considerations on the photocatalytic H2 evolution performance of Cu-doped TiO2 obtained by different doping methods.* ACS Catalysis, 2014. **4**(10): p. 3320–3329.
3. Wei, T., et al., *Defect Modulation of Z-Scheme TiO2/Cu2O Photocatalysts for Durable Water Splitting.* ACS Catalysis, 2019. **9**(9): p. 8346–8354.
4. Lee, B.-H., et al., *Reversible and cooperative photoactivation of single-atom Cu/TiO2 photocatalysts.* Nature materials, 2019. **18**(6): p. 620–626.
5. Li, G., et al., *Highly Active Photocatalyst of Cu2O/TiO2 Octahedron for Hydrogen Generation.* ACS Omega, 2019. **4**(2): p. 3392–3397.
6. Wan-Ting, C., et al., *Effect of alcohol sacrificial agent on the performance of Cu/TiO2 photocatalysts for UV-driven hydrogen production.* Applied Catalysis A: General, 2020. **602**: p. 117703.
7. Sadanandam, G., et al., *Cu oxide quantum dots loaded TiO2 nanosheet photocatalyst for highly efficient and robust hydrogen generation.* Applied Surface Science, 2021. **541**: p. 148687.

8. Ma, Y., et al., *Highly enhanced photocatalytic hydrogen evolution activity by modifying the surface of TiO2 nanoparticles with a high proportion of single Cu atoms.* Catalysis Science & Technology, 2022. **12**(12): p. 3856–3862.
9. Xing, C., et al., *Synergistic effect of surface oxygen vacancies and hydroxyl groups on Cu-doped TiO2 photocatalyst for hydrogen evolution.* Materials Today Nano, 2023. **24**: p. 100435.
10. González-Tejero, M., et al., *High-performance photocatalytic H2 production using a binary Cu/TiO2/SrTiO3 heterojunction.* ACS Applied Energy Materials, 2023. **6**(7): p. 4007–4015.
11. Hu, J., et al., *Highly dispersed Cu 2 O quantum dots (about 2 nm) constructed by a simple functional group anchoring strategy boost the photocatalytic water splitting ability by 72 times.* Journal of Materials Chemistry A, 2023. **11**(3): p. 1290–1300.
12. Zi, B., et al., *Changeable Active Sites by Pr Doping CuSA-TiO2 Photocatalyst for Excellent Hydrogen Production.* Small, 2024. **20**(27): p. 2305779.
13. Xu, S., et al., *Highly efficient CuO incorporated TiO2 nanotube photocatalyst for hydrogen production from water.* International Journal of Hydrogen Energy, 2011. **36**(11): p. 6560–6568.
14. Muscetta, M., et al., *Hydrogen production through photoreforming processes over Cu2O/TiO2 composite materials: A mini-review.* International Journal of Hydrogen Energy, 2020. **45**(53): p. 28531–28552.
15. Cargnello, M., et al., *Photocatalytic H2 and added-value by-products–the role of metal oxide Systems in Their Synthesis from oxygenates.* European Journal of Inorganic Chemistry, 2011. **2011**(28): p. 4309–4323.
16. Kennedy, J., et al., *Hydrogen production by the photoreforming of methanol and the photocatalytic water–gas shift reaction.* Journal of Physics: Energy, 2021. **3**(2): p. 024007.
17. Pai, M.R., et al., *A comprehensive study on sunlight driven photocatalytic hydrogen generation using low cost nanocrystalline Cu-Ti oxides.* Solar Energy Materials and Solar Cells, 2016. **154**: p. 104–120.
18. Yoong, L., F.K. Chong, and B.K. Dutta, *Development of copper-doped TiO2 photocatalyst for hydrogen production under visible light.* Energy, 2009. **34**(10): p. 1652–1661.
19. Kresse, G. and J. Furthmüller, *Efficiency of ab-initio total energy calculations for metals and semiconductors using a plane-wave basis set.* Computational materials science, 1996. **6**(1): p. 15–50.
20. Maniopoulou, A., et al., *Introducing k-point parallelism into VASP.* Computer Physics Communications, 2012. **183**(8): p. 1696–1701.
21. Gajdos, M., et al., *Electronic structure: Wide-band, narrow-band, and strongly correlated systems-Linear optical properties in the projector-augmented wave methodology.* Physical Review-Section B-Condensed Matter, 2006. **73**(4): p. 45112–45112.
22. Perdew, J.P., et al., *Atoms, molecules, solids, and surfaces: Applications of the generalized gradient approximation for exchange and correlation.* Physical review B, 1992. **46**(11): p. 6671.
23. Ernzerhof, M. and G.E. Scuseria, *Assessment of the Perdew–Burke–Ernzerhof exchange-correlation functional.* The Journal of chemical physics, 1999. **110**(11): p. 5029–5036.
24. Ling, C., et al., *Nanosheet supported single-metal atom bifunctional catalyst for overall water splitting.* Nano letters, 2017. **17**(8): p. 5133–5139.